Oxid Met (2018) 90:365–381
https://doi.org/10.1007/s11085-018-9845-6

ORIGINAL PAPER

Impact of Deposits and Their Morphology on the Active Corrosion of Iron in Chlorine- and Sulfur-Containing Atmospheres in the Temperature Range of 350–500 °C

Ludmila Krumm[1] · **Mathias C. Galetz**[1]

Received: 16 November 2017 / Revised: 3 March 2018 / Published online: 24 March 2018

Abstract Iron-based alloys have shown high corrosion rates under ash deposits typical for waste-to-energy plants. The ashes on superheater tubes in waste incineration are multicomponent systems including alkali and alkali–earth chlorides and sulfates. Under and within such salts, the corrosive effect on the alloy is induced by a complicated interplay of such ash products. On the one hand, in chlorine-containing atmospheres iron-based alloys are believed to be attacked by the so-called active corrosion, including the formation of volatile corrosion products and their transformation into stable iron oxides. At the same time, they form complex scales, involving among other compounds iron sulfides, chlorides, and oxides. Thus, in order to directly investigate the influence of a deposit on the corrosion in waste-to-energy plants and to reproduce the scales observed on field tested superheaters, this work compares the scale formation and metal wastage under different chemically inert alumina deposits with different grain sizes to a synthetic salt as well as to an actual deposit taken from a superheater tube in a plant.

Keywords Chlorine corrosion · Carbon steel · Waste incineration · High temperature · Deposits

Introduction

With increasing waste generation, the demand for reliable and more efficient waste-to-energy (WTE) plants grows worldwide [1]. The chlorine and the alkali chlorides in the combustion atmosphere pose a particular challenge to engineers and

✉ Ludmila Krumm
galetz@dechema.de

[1] Dechema-Forschungsinstitut (DFI), Theodor-Heuss-Allee 25, 60486 Frankfurt am Main, Germany

researchers [2–6]. Particularly, accelerated corrosion of superheater tubes is observed, which usually are made of carbon steel because the experience with more expensive solutions so far often does not justify their much higher cost. A typical corrosion scale found on low-alloyed field-returned superheater tubes is described in [7, 24]. Directly on the metal tube interface, they detected an iron chloride scale with FeS, followed by mixed iron oxides of hematite and magnetite. Between those scales Miller et al. found a red hematite powder layer. Other authors describe this Fe_2O_3 powder as pseudomorphic hematite crystals [8]. The presence of FeS and metal chlorides within the corrosion products under porous oxides indicates a low oxygen partial pressure ($p(O_2)$). In addition to the consumption of oxygen to form oxides, the deposits themselves can significantly contribute to a low $p(O_2)$. Deposits found on superheater tubes are usually composed of alkali and alkali–earth chlorides and sulfates [9], and mixtures of these compounds are used as fluxing agents in metallurgy in order to prevent melt oxidation [10]. Grabke and Reese showed in their work that solid chlorides are able to attack the oxide scale of metal samples and to release gaseous chlorine [11, 12]. This chlorine can diffuse to the metal surface to build volatile metal chlorides. On its way outward through the oxide scale, metal chlorides oxidize in areas with higher oxygen partial pressure by releasing chlorine, which can return back to the metal surface to induce accelerated corrosion by this cyclic process. This mechanism is well known as "active oxidation" [13, 14]. Furthermore, metal oxides formed during this process are porous and badly adhered, so they do not serve as protective scale. A further source for chlorine can also be sulfation processes (reaction 1) as it was suggested in the study by P.D. Miller and H.H. Krause in [15]:

$$4NaCl + SO_2 + O_2 + 2H_2O \leftrightarrow 2NaSO_4 + 4HCl \quad (1)$$

Additionally, a corrosive attack can be caused by molten salts. Some chloride salt mixtures containing heavy-metal compounds have a low melting point, e.g., 48ZnCl2-52KCl at 250 °C [1]. Such molten salts dissolve the tube material and protective scales and thus enhance the corrosion attack strongly already at low temperatures. All laboratory investigations on this topic, e.g., by Kawahara [16], Ishitsuka et al. [17], Brossard [18], or Bauer [19], used an oxygen-rich (several % O_2) flue gas and usually observed such dissolution reactions as the dominant corrosion mechanisms.

In this work, as a novel approach to reproduce the corrosion products that are observed on field-returned low-alloyed steels [7, 24] in the laboratory is suggested. It is important to understand and be able to simulate the local conditions under a think "living" deposit (with temperature gradient, condensating species such as KCl etc.). The impact of oxygen partial pressure as well as of deposits, inert ones (that allow to separate chemically and physical influence on the corrosion rate in chlorine-containing atmospheres) as well as typical WTE deposits was examined.

Experimental Procedures

In the first part, tests with and without Al_2O_3 powder deposits were performed in the temperature range between 350 and 500 °C for 300, 600, and 900 h in chlorine- and sulfur-containing atmospheres with high and low oxygen partial pressure. Alumina was selected as it is thermodynamically inert compared to iron as well as in contact with the testing atmosphere. An atmosphere with a high oxygen partial pressure was chosen as a typical waste-to-energy (WTE) plant atmosphere [Prewin Guideline European network on Performance, Reliability and Emissions Reduction in Waste Incinerators] containing 0.1 vol%HCl + 0.01 vol%SO_2 + 8 vol%O_2 + 17 vol%H_2O + 10 vol%CO_2 + N_2 balance (hereinafter referred to as synthetic WTE plant atmosphere). In addition, an atmosphere with low oxygen partial pressure was selected to simulate the condition under deposits which had the same HCl and SO_2 content (0.1 vol% each) but considerably less O_2 at 15ppmO_2 (N_2 balance). CO_2 was neglected. For each parameter combination, two samples were exposed. The raw material used for all tests in this work was the carbon steel 16Mo3, typically used for superheater tubes in boiler. It was delivered by a commercial supplier (Quick Metall) as rods. Its nominal and actual chemical composition as a mean of five measurements by OES (Optic spark emission spectrometer; SPECTROMAXx) is given in Table 1. In addition to the specified elements, only Cu was present at a significant amount of 0.16% (all others < 0.01). The rods had a diameter of 8 mm and were cut into pieces of 15 mm in length. Afterward, the cylindrical samples were ground by using a 400-grit abrasive paper and finally cleaned in ultrasonic bath with ethanol.

Before testing the samples were measured and weighed, and each sample was placed separately in an alumina crucible. The weight of the samples including the crucibles and the weight of samples placed in crucibles including the alumina powder deposit were determined. An alumina powder (delivered by Carl Roth chemicals) was used, in which 30% of the alumina grains are smaller than 63 μm, while grains around 100 μm represent the major share of the powder. In the first part of this investigation, the coverage level for all tests with alumina powder deposit was 10 mm above the top of the sample surface. In the second part of this work, the impact of the grain size and of the coverage level of the alumina deposit was investigated. A fine alumina powder (Amperit 740, grain size < 5 μm delivered by H.C. Starck) and a coarse alumina powder (∼ 100 μm) were compared to the aforementioned alumina powder deposit. In the following the different salt types will be referred to as deposit type 3 (< 5 μm), deposit type 2 (∼ 100 μm), and

Table 1 Chemical composition of carbon steel 16Mo3 (1.5415)

Element (mass%)	C	Ni	Mn	Cr	Mo	Si	Al
Nominal	0.12–0.2	≤0.3	0.4–0.9	≤0.3	0.25–0.35	≤0.35	≤0.04
Actual	0.17	0.09	0.69	0.19	0.28	0.27	0.02

deposit type 1 (63–100 µm). Two coverage levels were used: 2 and 10 mm above the top of the sample. Finally, in order to compare the influence of such chemically inert alumina deposits to active salts, a synthetic salt of 5 wt% NaCl, KCl, Na_2SO_4, K_2SO_4 and 80 wt% $CaSO_4$ as proposed by [20] was used in crucibles as well as one deposit from an actual WTE superheater; for both the two different coverage levels were used.

After exposure, all samples were weighed including the crucible and, in the case of covered samples, including the alumina powder. Mass change was determined by the weight difference before and after exposure. Then one sample of each parameter combination was prepared for metallographic examination, and another was used for quantification of the material wastage. All cross sections were prepared water-free as described in [21] and analyzed by light optical microscopy (LOM), scanning electron microscopy (SEM), and electron probe microanalysis (EPMA). Material wastage was estimated by mass change determination after the corrosion products were removed. For this purpose, samples were exposed in an HCl solution containing an inhibitor as described in [22]. Here the samples were weighed several times during etching, whereby during the first 20 min most corrosion products were removed. The procedure of corrosion product removal was finished when the mass change after several measure steps was smaller than 0.5 mg/cm^2. Depending on corrosion scale thickness, the etching process took no longer than 2 h. In comparison, an untreated sample loses around 0.2 mg/cm^2 after an hour of treatment.

On several samples, the distribution of corrosion products formed in the vicinity of the surface was measured using an optical software tool (IMS).

Results and Discussion

Impact of Chemically Inert Al_2O_3 Powder Deposit on Corrosion Rates

In Fig. 1 the results of material wastage from the tests in low oxygen 0.1%HCl + 0.01%SO_2 + 15ppmO_2 + N_2 balance and in synthetic WTE plant atmosphere with and without Al_2O_3 powder deposit are compared. Interestingly, in synthetic plant atmosphere no impact of the inert deposit on the corrosion rate of 16Mo3 could be observed (Fig. 1a) and the inherent oxidation of the substrate dominates the corrosion process. The material wastage is even comparable to that for air oxidation data summarized [34] and discussed in [35]. In high oxygen partial pressure the influence of chlorine and active oxidation can be neglected [35] in line with [36]. In contrast, in the low oxygen atmosphere the material wastage increased under Al_2O_3 with this effect being most pronounced at 380 and 440 °C (Fig. 1 b). At higher temperatures this effect on the corrosion rate was lower again.

In such cases, where the alumina deposit had an impact on the corrosion rate, the alumina was colored gray in the vicinity of the sample surface after exposure. Furthermore, the colored alumina powder was sticking to the samples (Fig. 2a). Such gray particles in the alumina deposit must have been built via gas phase reactions and could be identified by SEM and EDX examination as crystalline iron

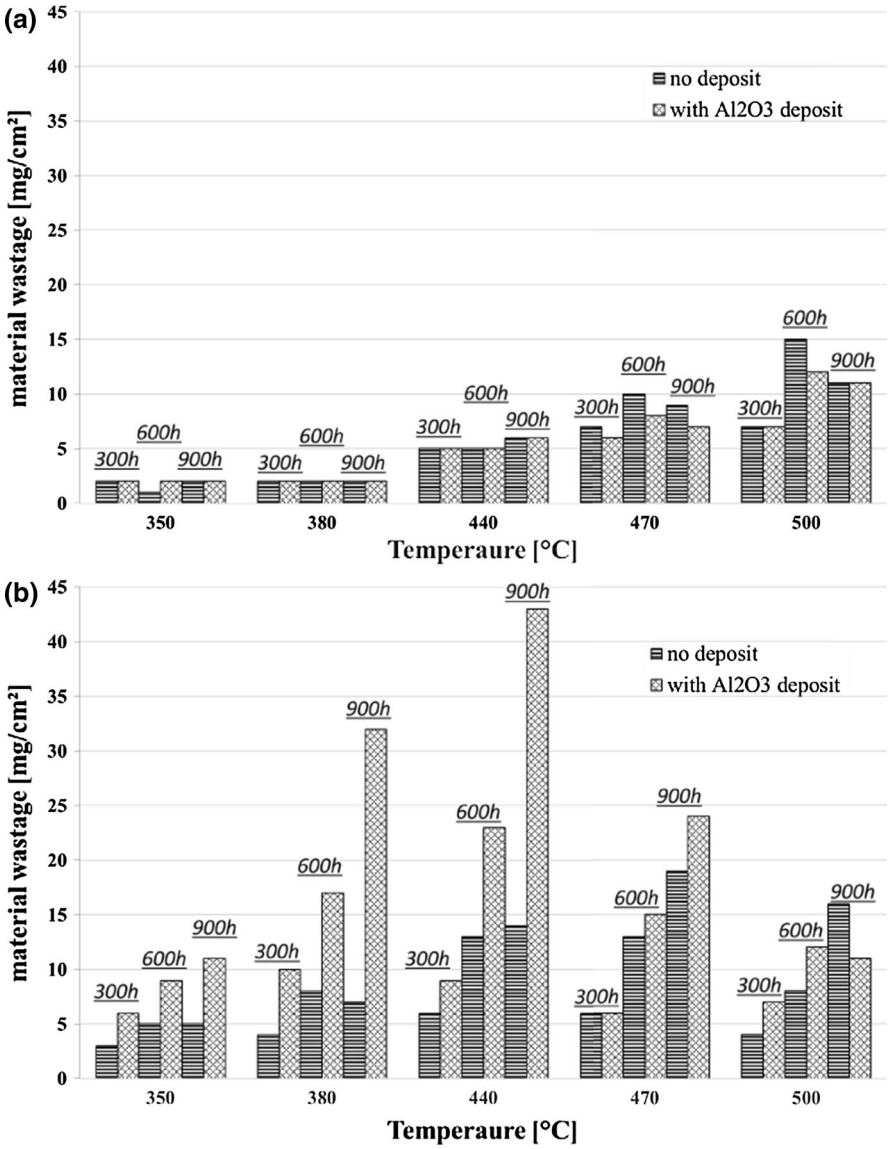

Fig. 1 Effect of Al_2O_3 powder deposit on material wastage as a function of exposure temperature and time in **a** synthetic WTE plant atmosphere and **b** 0.1%HCl + 0.01%SO2 + 15ppmO2 + N2 balance

oxides with an iron-to-oxygen ratio of approximately 2:3 as shown in Fig. 2b). A detail SEM image of such crystals is represented in Fig. 3.

Therefore, in the atmosphere with low oxygen partial pressure, chlorine and its volatile corrosion products dominate the corrosion process and are most important for the corrosion mechanisms especially in the considered temperature range of WTE plants around 400 °C (Fig. 1b). In accordance with McNallan et al.'s model of

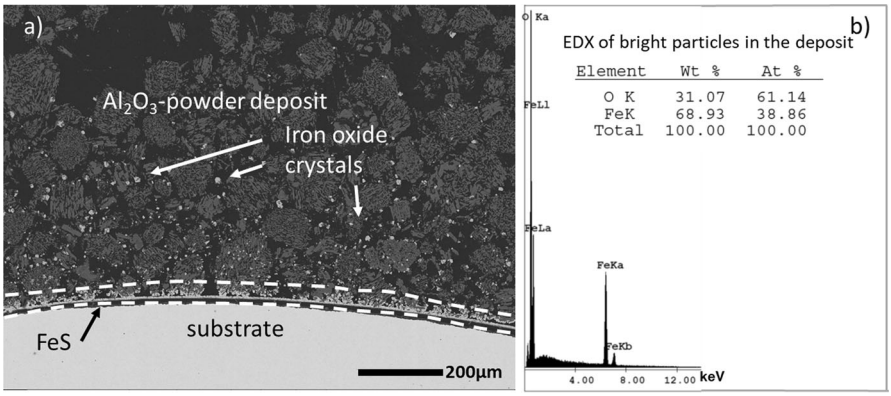

Fig. 2 **a** SEM picture of alumina powder 1 and corrosion products after 300-h exposure in $0.1\%HCl + 0.01\%SO_2 + 15ppmO_2 + N_2$ balance atmosphere at 440 °C. **b** EDX result of a crystalline corrosion product in alumina powder

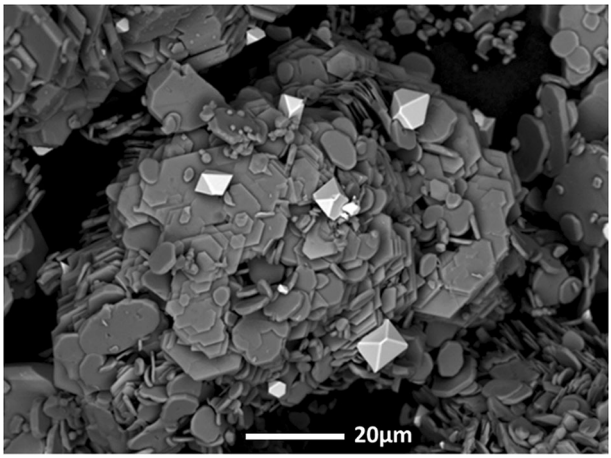

Fig. 3 SEM image of octahedron-shaped iron oxide crystals (bright particles) on an Al_2O_3 powder particle

active oxidation described in [13], the volatile chlorides can oxidize on their way from the sample surface to the fluent gas atmosphere to form the observed "gray" oxide particles in the alumina deposit. In the process they release the chlorine because thermodynamics dictate (Fig. 4) that at some point the metal chlorides have to react with the oxygen molecules when the oxygen partial pressure increases further away from the metal.

The more often or more likely it is that such chlorides "see" oxygen, the more probable is their oxidation. Since the porosity is very high in the deposits, Knudsen diffusion does not play a role and the gas transport should not affected. Still, in our tests, the alumina powder deposit serves as an obstacle for the volatile iron chlorides on their way out, which can adsorb on the alumina surface to react and nucleate the

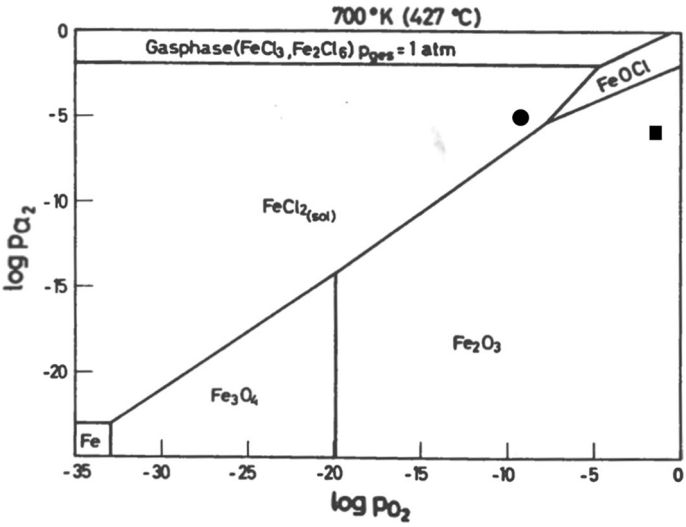

Fig. 4 Phase stability diagram at 427 °C for iron in an environment containing O_2 and Cl_2, reproduced with permission from [14]. The circle and the square mark the atmospheres used in this work 0.1%HCl + 0.01%SO_2 + 15ppmO_2 + N_2 and synthetic WTE plant atmosphere, respectively

oxides. Thus, dwell time of the iron chloride close to the sample surface increases due to the interaction with the deposit particles and therefore also the likelihood of their oxidation near to the sample surface, compared to tests without deposit. Further research is required to reveal the exact mechanism of oxide formation in the deposit, where heterogeneous nucleation of the iron oxides on deposit particles might play a role. However, what is clear is that if the quantity of oxidized iron chlorides under the deposit increases, the chlorine is set free close to the surface and the chlorine partial pressure increases to enhance the corrosion attack, as described in the active oxidation model.

With increasing temperatures, the vapor pressure of iron chloride increases, see [23]. At 470 and 500 °C much less grayish particle deposition or iron oxide, respectively, was found in the deposits. $FeCl_2$ becomes volatile and remains metastable to pass the particles of the deposit without being transformed into oxides. Oxidation occurs somewhere toward the outlet of the furnace in this case, so that no increase in p(Cl_2) under the deposit will be induced. Thus, there is a much lower effect of the inactive alumina deposit on the corrosion rate at higher temperatures in low chlorine-, low oxygen-containing atmospheres.

Influence of Grain Size and Coverage Level of Alumina Powder Deposit on Corrosion Rate

Based on the results in the atmosphere with low oxygen partial pressure, further tests at 440 °C were conducted, as the highest impact of deposit on corrosion rates was observed at this temperature. For this investigation of the particle grain size and the amount of alumina, an exposure time of 300 h was used. The resulting mass

change and material wastage with all three alumina powder deposit types are comparable as presented in Figs. 5 and 6, respectively, and are independent of the coverage level. Interestingly, at the same time, the morphology and distribution of the corrosion products differ significantly (Fig. 7).

As shown in Figs. 2 and 3, small iron oxide crystals are formed and are finely distributed within the alumina deposit. Under the 63–100 µm powder, the transformation from chlorides to oxides took place for up to a maximum distance of 500 µm from the substrate surface (Fig. 7a). Comparable behavior was observed with the deposit consisting of 100 µm grain-sized alumina powder (Fig. 7b). This situation changes with the fine-grained alumina powder deposit (Fig. 7c). In this case, a rather dense iron oxide scale of large crystals formed close to the sample surface, and the measured average maximum path length of the chlorides up to their transformation into oxides was only 150 µm. Due to the fine-grained structure of the deposit, the particles offer a much higher surface area for adsorption and nucleation. In addition, the channels for the outward diffusion of the chlorides are narrower than for the other two alumina deposit types so they get filled by the corrosion products close to the surface. The distance of the chlorides covered before they transform to oxides is in all cases smaller than the applied deposit thickness levels used in this work. Thus, no strong effect of the deposit thickness level on corrosion rates was observed. In contrast, as all iron chlorides are transformed within the deposits and release their chlorine, there is a high chance that chlorine returns to the metal and reacts again, which can explain the higher corrosion rates in all cases with deposit due to active oxidation.

Chemically, the corrosion products are very similar with all three alumina deposit types. Very close to the metal the corrosion products are not oxides; instead, the corrosion scale consists of iron- and chlorine-rich scale followed by iron sulfide FeS

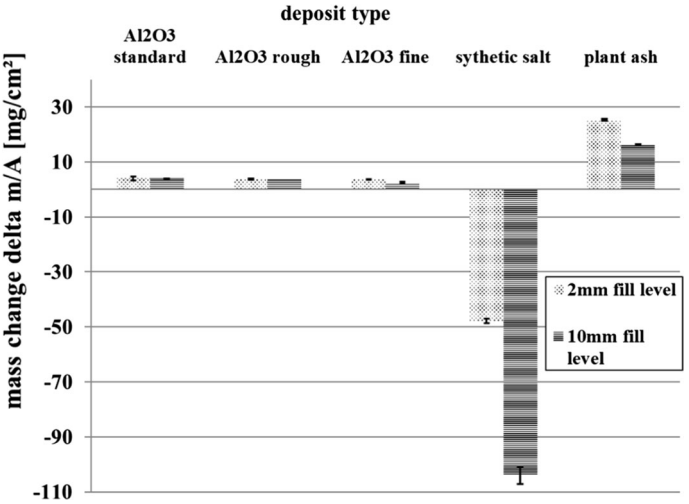

Fig. 5 Mass change as a function of deposit type and coverage level at 440 °C after 300-h exposure in 0.1%HCl + 0.01%SO_2 + 15ppmO_2 + N_2 balance atmosphere

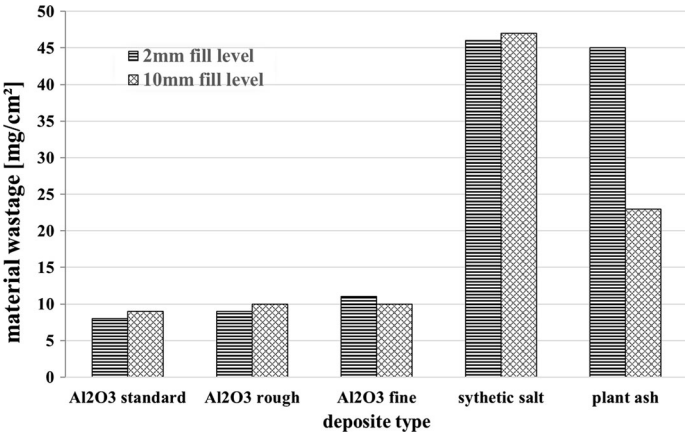

Fig. 6 Material wastage as a function of deposit type and coverage level at 440 °C after 300-h exposure in 0.1%HCl + 0.01%SO_2 + 15ppmO_2 + N_2 balance atmosphere

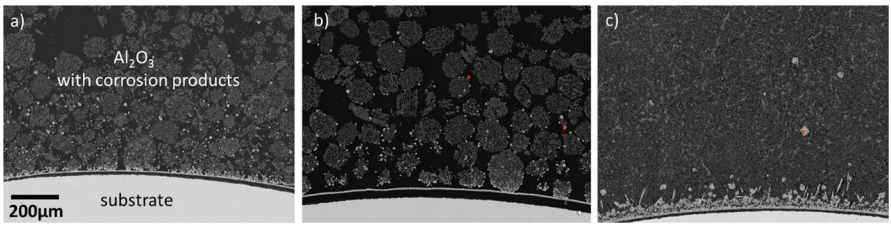

Fig. 7 SEM picture of three different alumina powder deposits after 300-h tests in 0.1%HCl + 0.01%SO_2 + 15ppmO_2 + N_2 balance atmosphere at 440 °C. **a** 63–100 µm Al_2O_3 (type 1) **b** ~ 100 µm grained Al_2O_3 (type 2), and **c** < 5 µm grained Al_2O_3

as exemplarily shown in the EPMA line scan for the standard Al_2O_3 powder in Fig. 8a) and selected element distribution maps (Fig. 8b). Above this scale, the iron oxide crystals are found as shown above.

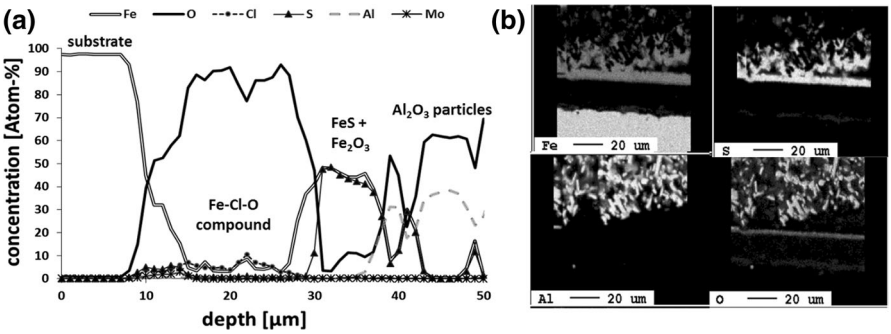

Fig. 8 **a** Line scan with **b** EPMA element distribution maps showing the substrate/corrosion scale interface of 16Mo3 exposed in 0.1%HCl + 0.01%SO_2 + 15ppmO_2 + N_2 at 440 °C for 300 h and covered with Al_2O_3 powder deposit

The formation of FeS is typical for WTE corrosion scales, and it occurs at low oxygen partial pressures close to the metal [7, 24]. It indicates that SO_2 (which remains stable over SO_3 in this temperature range and atmosphere as calculated via FactSage (not shown here)) dissociates like described elsewhere [25]. The released sulfur and oxygen then react with iron or with iron compounds. It can be assumed that, in systems with a low oxygen partial pressure, SO_2 can serve as an oxidant instead of O_2 during active oxidation. Interestingly, no oxygen-containing corrosion products coexist with the FeS, but oxygen is measured simultaneously with iron chlorides. According to this observation, one possibility is the formation of oxychlorides FeOCl. This compound was described before to occur in this temperature range in [14, 26]. Oxychlorides behave similar to chlorides, being volatile and transformed into oxides further away from the metal as shown by A.W. Henderson [27]. A sum of possible reactions can be described by reactions 2–4:

$$3FeCl_2 + SO_2 = 2FeOCl + FeS + 2Cl_2 \quad (2)$$

$$3FeOCl = Fe_2O_3 + FeCl_3 \quad (3)$$

$$4FeOCl + O_2 = 2Fe_2O_3 + 2Cl_2 \quad (4)$$

Such reactions can also explain why the crystals often have some FeS on the surface (reaction 2).

Another aspect which should be discussed in more in detail is the nature of the iron oxide crystals found. As described in Fig. 2b), EDX measurements of the crystals indicate hematite, but its cubic structure is typical for magnetite. Also Reichel describes in his work these corrosion products as pseudomorphic hematite crystals originating from magnetite [8]. These observations suggest that these crystals are—or were—maghemite. Since it is clear that they formed by a "chemical vapor deposition process" at increased oxygen partial pressures compared to that at the metal surface, this finding is in good agreement with the fact that maghemite is an oxygen-deficient metastable Fe(III) oxide (Fe_2O_3) and has the same spinel ferrite structure as magnetite. For this reason, maghemite is difficult to distinguish from magnetite using common analysis methods such as XRD. Thus, further investigation was needed in order to clarify the nature of the present iron oxide crystals.

Results of Exposure in Synthetic Salt Deposit and Its Comparison to the Inactive Alumina and Plant Deposit

Finally, mass change and material loss in the synthetic salt and plant salt are compared to the reactions occurring under the inactive alumina deposits. From Fig. 5, it becomes clear that the samples covered with synthetic salts largely increased mass change indicating strong corrosive attack. Another big difference is that the samples do not show a weight gain, but large weight loss. This means that evaporation processes dominate the behavior and large amounts of volatile species are not transformed into stable corrosion products within the deposits. Furthermore, there is an impact of coverage level on mass change. Samples with a coverage level

of 10 mm show double the mass loss compared to samples with a coverage level of 2 mm (Fig. 5). However, if the metal wastage is compared, the influence of the coverage level disappears suggesting that species such as KCl or KOH contribute to the evaporation. Substrate wastage at both coverage levels is around 0.046 g/cm^2 or about 60 µm and therefore *six times* higher than that observed in tests with alumina powder deposits. The increase in material wastage on samples exposed in synthetic salt could be related to an additional source of chlorine in the form of potassium chlorides in the salt. In the present tests the amount of synthetic salt per substrate area was 0.39 and 0.72 g/cm^2 for 2 mm and 10 mm coverage levels, respectively. Against this theory can be held the fact that the coverage level does not influence the mass loss rate, which suggests that the amount of chloride is not directly related to the material consumption. This means that above a certain chlorine amount the corrosion rate is not a function of $p(Cl_2)$ anymore. This finding is in agreement with Grabke et al. [28], who showed that the variation of the NaCl amount applied on a constant area did not affect the corrosion rate. A visible color change of the synthetic salt after exposure is observed.

The colorations are symmetrically distributed in ring shape around the cylindrical specimen (see Fig. 9b). It shows, again, gray color next to the sample surface and red color in outer scale. At 10 mm coverage level, some salt had to be removed from the surface until a red-colored salt emerged. In a distance of around 2 mm from the sample surface, the salt is strongly sintered at both coverage levels. Regions of salt which are more than 2 mm away from the metal have hardly changed their color and powdery appearance (Fig. 9a). Around the specimen a gray ring extends up to $\sim$ 700–800 µm from the metal surface. It is slightly further away from the metal interface than in the case of coarse-grained alumina deposits ($\sim$ 500 µm) and consists of similar iron oxide crystals as were found in alumina powder deposit. In the SEM picture presented in Fig. 10, this area is visualized by a bright outer ring. Additionally, EDX measurements in the different areas summarized in Table 2 show that up to 4 at% Fe were detected in the gray-colored region of the salt. Outside the colored area, the iron amount reaches a maximum of 1 at%. Furthermore, in the outer transition area at about 2 mm between colored and

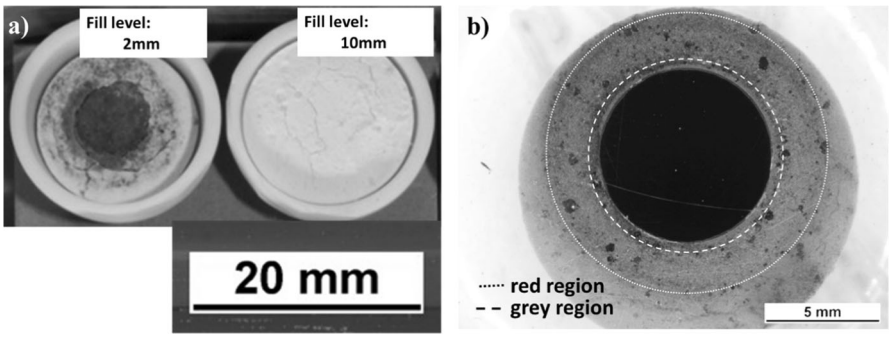

Fig. 9 16Mo3 after 300 h of exposure in synthetic salt (5 wt% NaCl, KCl, Na_2SO_4, K_2SO_4 and 80 wt% $CaSO_4$) in the atmosphere 0.1%HCl + 0.01%SO_2 + 15ppmO_2 + N_2 balance at 440 °C **a** state direct after exposure in crucible and **b** metallographically prepared cross section

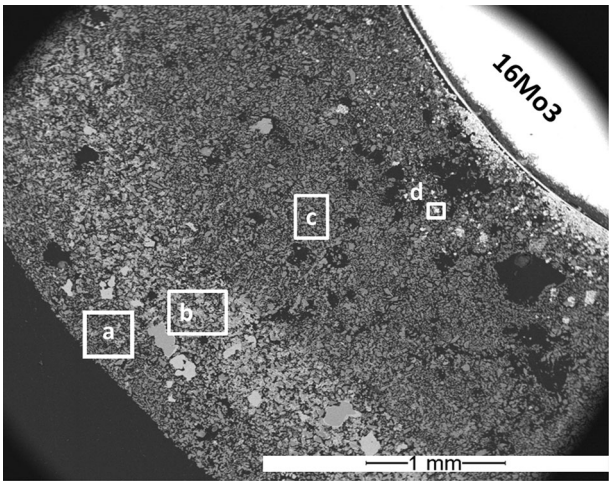

Fig. 10 SEM cross section of 16Mo3 with synthetic salt deposit after 300-h exposure at 440 °C in 0.1%HCl + 0.01%SO_2 + 15ppmO_2 + N_2 balance atmosphere

Table 2 Elemental composition of selected areas (see Fig. 10) of corrosion products and deposits after exposure of 16Mo3 in synthetic salt at 440 °C for 300 h in 0.1%HCl + 0.01%SO_2 + 15ppmO_2 + N_2 balance

Region	Elemental composition (at%)						
	O	Na	S	Cl	K	Ca	Fe
a	60.2	4.4	15.2	4.5	1.9	11.3	1.8
b	51.7	3.9	9.5	14.6	8.5	7.6	4.3
c	62.3	1.6	16.6	2.0	–	13.3	4.2
d	58.0	–	–	–	–	–	42.4

uncolored salt, the amount of potassium is strongly increased compared to the other analyzed areas in the deposit. This potassium plus sodium is slightly lower than the Cl content, suggesting that all alkalis are present as chlorides in this zone.

Another indication for this assertion is that the "red" area particles consist of NaCl-KCl salt mixtures with a eutectic morphology as shown in Fig. 11 as well as the accumulation of potassium at the right side of the map in a spot where oxygen is not measured at all. In contrast, the results of Schaal [20] using the same salt indicate that below 510 °C no molten phase should be present in the salt. One possibility to decrease the melting point was by third compounds such as $FeCl_2$ which are able to form eutectics. $FeCl_2$ was not measured within the eutectic structured particle shown in Fig. 9, but even traces below the detection limit of the EPMA can have a significant effect because it can lower the melting point if mixed with both KCl and NaCl salt mixtures to 355 and 370 °C, respectively [29].

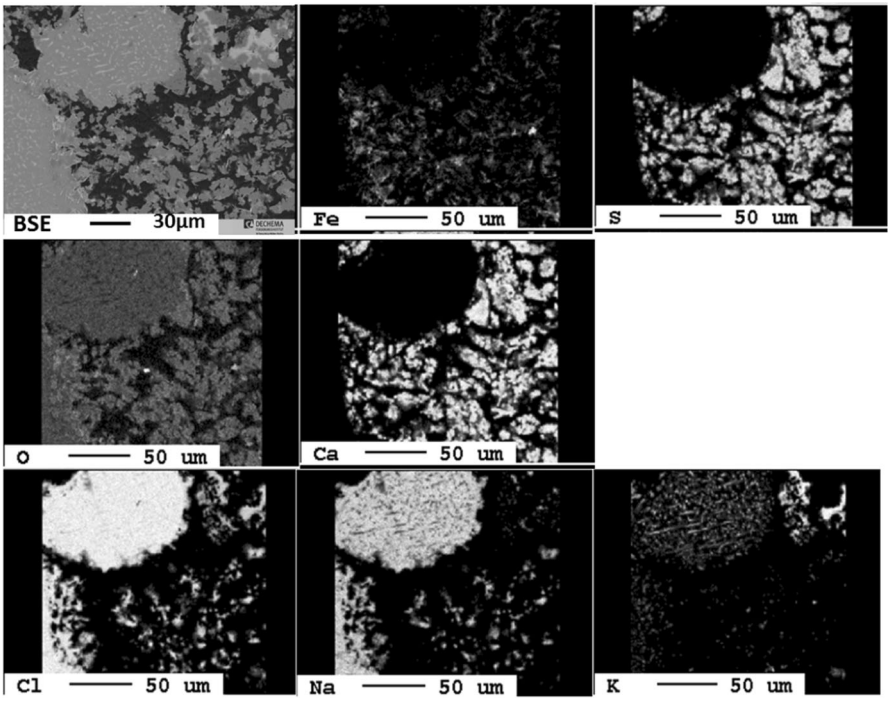

Fig. 11 BSE and element maps of synthetic salt compounds after exposure at 440 °C in 0.1%HCl + 0.01%SO_2 + 15ppmO_2 + N_2 balance atmosphere for 300 h

Comparable to the test with inactive deposits, samples exposed in synthetic salt also exhibit a FeS corrosion scale next to the metal surface (Fig. 12). It is notable that NaCl and KCl are found deep within the corroded scale down to the metal surface, while, e.g., Ca-containing compounds, which are also a strong chloride formers, are only located in the deposits further away from the sample surface. Liquefaction or high vapor pressures of alkali chlorides in contrast to earth–alkali chlorides can explain the difference in the mobility of such species. The aggressiveness of KCl in contact with iron was extensively studied in several publications [20, 30, 31].

Surprisingly, the "fully reacted" plant salt also shows a very similar metal wastage as the synthetic salt although, instead of a mass loss, again a mass gain is observed. This shows that the trace elements most significant for the corrosive attack on the metal species are still present in an aged ash, in which most alkali and earth–alkali species should have been sulfurized [15]. Interestingly, the composition of the corrosion scale and the enrichment of NaCl and KCl within the corrosion scale at the metal surface are comparable as well to the other results. However, the samples exposed in plant salt with the higher fill level show a different behavior. Not only is their mass change only half, also their material wastage is less compared to the samples with the fill level of 2 mm. However, some extraordinary observations were made on these samples. The plant salt was strongly sintered. In

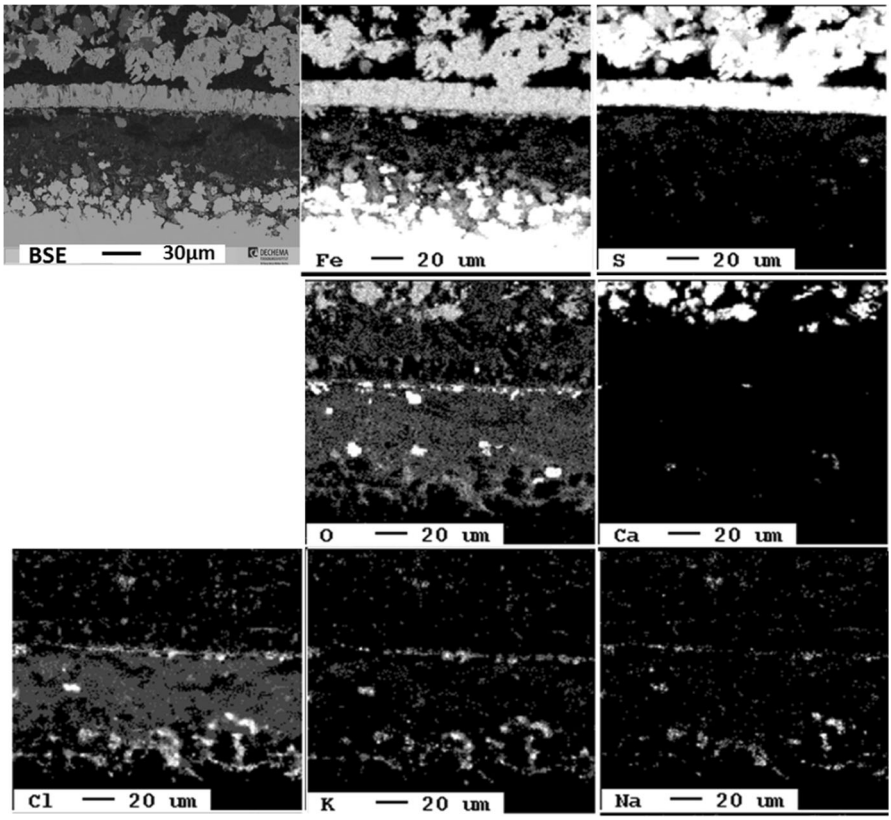

Fig. 12 Cross section and element maps of metal/corrosion scale interface of a sample exposed in synthetic salt at 440 °C for 300 h in 0.1%HCl + 0.01%SO_2 + 15ppmO_2 + N_2 balance atmosphere

order to reach the sample, the deposit had to be broken open. Furthermore, the cross section released a large amount of chlorine, which reacted immediately with the freshly polished surface. Consequently, a reliable analysis of the corrosion products was not possible in this case. However, this shows that the salt becomes so dense that it limits the exchange with the gas, which in retrospect confirms the assumption of a low oxygen partial pressure under WTE superheater deposits and approves the approach to test under the proposed atmosphere used for the tests here. Hence, after consumption of the available oxygen under the deposit, the further corrosion process was reduced due to a lack of gas exchange, explaining the lower material consumption shown in Fig. 5b. In conjunction, the kinetics of the corrosion reaction changes. The rate-determining step is not volatilization and transformation of iron chlorides anymore. Not only the external gas cannot penetrate through the sintered deposit, also the formed gaseous chlorides are hindered to diffuse into the fluent gas. Thus, an iron chloride scale can form on the substrate surface which would explain the massive chlorine release during preparation [32].

The stronger sintering in plant salt in comparison with the synthetic salt can be ascribed to the additional elements contained in plant salts such as Ni, Si, Al, or Cu. Some of these elements are even able to catalyze the corrosion reactions under the deposit as reported in [19]. The sample with the lower coverage level does not develop a dense cover layer due to sintering in comparison with the sample with the thick deposit. Thus, the gas exchange can take place, and the metal wastage is similar to the one observed under synthetic salts.

Conclusions

The aim of this study was to investigate the impact of active and inert deposits and the local atmosphere close to a WTE superheater tube at the metal surface and on the induced corrosive attack on carbon steel 16Mo3 in hydrogen chloride- and sulfur dioxide-containing atmospheres. In this approach, the influence of coverage level and grain size of different inert and chemically active deposits was investigated at different oxygen partial pressures. Finally, the results were compared to tests in synthetic salt deposit and to tests with deposits from an actual WTE plant. The corrosion tests were performed in the temperature range between 350 and 500 °C.

In atmospheres with high oxygen partial pressure (8% O_2), no change in corrosion rates was observed on samples covered with alumina powder deposit compared to samples exposed without deposit and the metal wastage was well in the range observed for simple air oxidation [34, 35].

However, a clear effect of alumina powder deposit on corrosion rates was observed in an atmosphere with low oxygen partial pressure, especially at lower temperatures up to 440 °C.

As active oxidation was confirmed as the main corrosion mechanism in this work in atmospheres with low $p(O_2)$, it can be concluded that the deposit accumulates chlorine after oxidation of iron chlorides and hinders their escape into the fluent gas. Thus, the $p(Cl_2)$ increases under the deposit with simultaneous increase in the corrosion rate. Further analysis of corrosion rates related to the powder properties coverage level and grain size showed that there was limited influence of these parameters. Most pronounced was an effect on corrosion scale morphology with very fine grain-sized alumina compared to coarser particles. While a scale of large iron oxide crystals adjacent to the metal scale was found under the fine-grained deposit, the coarse-grained powder led to the formation of small iron crystals dispersed widely within the deposit. Thus, the oxidation process took place at a certain distance from the surface.

After exposure in synthetic salts the attack increased by a factor of six, but the coverage level had no influence on the corrosion rate in atmospheres with low oxygen partial pressure, suggesting that the higher corrosion rate is not related to higher chlorine levels initially provided. Instead, enhanced NaCl and especially KCl amounts were found in deposits and in the vicinity of the metal, and they seem to play a very active role in the corrosion mechanism.

One conformity between inactive and synthetic deposit was the formation of FeS next to the metal surface, which has also been described for WTE superheaters [7, 24].

Results from tests on samples exposed in plant deposit with a low coverage level of 2 mm were found comparable to those obtained from tests with synthetic salts. In contrast, under a plant deposit with higher fill level, the corrosion rate was much lower compared to the lower fill level and to the tests in synthetic salt. Due to sintering of the salt, the exchange between the furnace atmosphere and the atmosphere under the deposit was limited, which retrospectively confirmed the occurrence of low oxygen partial pressures even above the corrosion products. Thus, the conditions at the scale interface between deposit and corrosion scale are completely different from those found at the interface deposit/fluent gas. Hohmann is to our knowledge the first one who suggested [33] gas transport restrictions due to reactions within the deposit and considers to strongly influence chlorine corrosion. Such findings are highly relevant for the testing of, e.g., alternative materials or new coatings to simulate the attack under WTE salts and ashes.

Acknowledgements Thanks are expressed to the Federal Ministry of Education and Research Germany (BMBF) for financing this work and to Ragnar Warnecke from GKS Schweinfurt for providing the plant ash.

References

1. Eurostat, *Environmental statistics and accounts in Europe,* http://ec.europa.eu/eurostat/de/web/products-statistical-books/-/KS-32-10-283 (2010).
2. S. Pollmann, *Chemie Ingenieur Technik* **39** (1967).
3. P. L. Daniel, L. D. Paul and J. Barna, *Materials Performance* **27**, 1988 (22).
4. Y. Kawahara, *Corrosion Science* **44**, 2002 (223).
5. P. Viklund, A. Hjörnhede, P. Henderson, A. Stålenheim and R. Pettersson, *Fuel Processing Technology* **105**, 2013 (106).
6. P. Mayer and A. V. Manolescu, *Corrosion* **36**, 1980 (369).
7. P. D. Miller, H. H. Krause, D. A. Vaughan and W. K. Boyd, *Corrosion* **28**, 1972 (274).
8. H.-H. Reichel, *Materials and Corrosion* **39**, 1988 (54).
9. K. Kautz and J. Tichatschke, *VGB Kraftwerkstechnik* **52**, 1972 (249).
10. D. Kopeliovich, *Fluxes for melting aluminum,* www.substech.com/dokuwiki/doku.php?id=fluxes_for_melting_aluminum (2012).
11. E. Reese and H. J. Grabke, *Materials and Corrosion* **43**, 1992 (547).
12. E. Reese and H. J. Grabke, *Materials and Corrosion* **44**, 1993 (41).
13. M.J. McNallan, W.W. Liang, S.H. Kim, and C.T. Kang, in *Proceedings of High Temperature Corrosion*, San Diego California, 2–6 March 1981, ed. by R.A. Rapp, NACE, 1983), p. 316.
14. O. Kubaschewski and I. Barin, *Pure and Applied Chemistry* **38**, 1974 (469).
15. P. D. Miller, H. H. Krause, J. Zupan and W. K. Boyd, *Corrosion* **28**, 1972 (222).
16. Y. Kawahara, *Materials at High Temperatures* **14**, 1997 (261).
17. T. Ishitsuka and K. Nose, *Corrosion Science* **44**, 2002 (247).
18. J. M. Brossard, I. Diop, X. Chaucherie, F. Nicol, C. Rapin and M. Vilasi, *Materials and Corrosion* **62**, 2011 (543).
19. M. C. Galetz, J. T. Bauer, M. Schütze, M. Noguchi, C. Takatoh and H. Cho, *Materials and Corrosion* **65**, 2014 (778).
20. E. Schaal, N. David, P. J. Panteix, C. Rapin, J. M. Brossard and F. Maad, *Oxidation of Metals* **84**, 2015 (307).
21. K. Rahts, M. Schorr, C. Schwalm and M. Schütze, *Praktische Metallographie* **36**, 1999 (86).

22. NACE International, *Preparation, Installation, Analysis, and Interpretation of Corrosion Coupons in Oilfield Operations* (2005).
23. R. Bender and M. Schütze, *Materials and Corrosion* **54**, 2003 (567).
24. B. Waldmann, Dr. rer. nat. Thesis, Universität Augsburg, 2007.
25. Z. Grzesik and S. Mrowec, *High Temperature Materials and Processes* **31**, 2012 (539).
26. H. Schäfer, *Zeitschrift für Anorganische und Allgemeine Chemie* **261**, 1950 (142).
27. A. W. Henderson, T. T. Campbell and F. E. Block, *Metallurgical Transactions* **3**, 1972 (2579).
28. H. J. Grabke, E. Reese and M. Spiegel, *Corrosion Science* **37**, 1995 (1023).
29. G. Sorell, *Materials at High Temperatures* **14**, 1997 (137).
30. M. Spiegel, *Materials and Corrosion* **50**, 1999 (373).
31. J. Pettersson, N. Folkeson, L.-G. Johansson and J.-E. Svensson, *Oxidation of Metals* **76**, 2011 (93).
32. R. J. Fruehan, *Metallurgical Transactions* **3**, 1972 (2585).
33. U. Hohmann, in Rauchgasseitige Dampferzeugerkorrosion: Erfahrungen bei der Schadensminderung, ed. by M. Born, Saxonia, (Freiberg, 2003), p. 79.
34. N. Bertrand, C. Desgranges, D. Poquillon, M. C. Lafont and D. Monceau, *Oxidation of Metals* **73**, 2010 (139).
35. L. Krumm and M. C. Galetz, *Oxidation of Metals* **87**, 2017 (757).
36. N. S. Jacobson, *Oxidation of Metals* **26**, 1986 (157).